Mineralogy and Petrology (1992) 47: 37–54

Mineralogy and Petrology

Evolution of PGE Mineralization in Hortonolitic Dunites of the Mooihoek and Onverwacht Pipes, Bushveld Complex

N. S. Rudashevsky[1], S. N. Avdontsev[2], and M. B. Dneprovskaya[3]

[1] Research-Analytic Complex, Mekhanobr; [2] All-Union Geological Research Institute; [3] Central Geological Exploration Museum, St. Petersburg, USSR

With 10 Figures

Received December 12, 1991
Accepted June 30, 1992

Summary

Platinum group minerals (PGM) and associated silicates, oxides and sulfides from four samples of platiniferous hortonolitic dunites of the Mooihoek and Onverwacht pipes, Bushveld Complex, show the following PGM assemblages: 1) (Pt, Fe) alloy similar to isoferroplatinum in composition, syngenetic with olivine; 2) sperrylite, syngenetic with clinopyroxene; 3) tetraferroplatinum, laurite, hollingworthite, unnamed mineral (Rh, Ru)AsS, syngenetic with titanomagnetite; 4) tetraferroplatinum (?), sperrylite, geversite, hollingworthite, platarsite, cabriite, rustenburgite, sobolevskite (?) and unnamed $(Pd, Pt)_4(Cu, Fe)_2(Sn, Sb)_3$, $(Pt, Ir)_3Sb$, (Rh, Ir, Pt)SbS, Rh(Sb, Bi)S, and Pt(Bi, Sb), syngenetic with late amphiboles, magnetite, chlorite, ilmenite, and pentlandite.

Fine (less than 0.1 mm) drop-like sulfide inclusions, consisting of troilite, ferruginous chalcopyrite, ferruginous pentlandite, and encircled by micrograins of magnetite, ilmenite, amphiboles, and biotite, were found in nonbroken grains of olivine. The inclusions' bulk composition is that of high-temperature sulfide phase in equilibrium with high-iron silicate melt, under conditions of low sulfur fugacity.

The temperatures at which different mineral assemblages were formed were studied in a sample of wehrlite, rich in titanomagnetite, and the following stages were identified: 1) a high temperature (980–1020 °C) stage measured using two-pyroxene thermometry; and 2) a high to medium temperature stage, measured using exsolution textures of titanomagnetite aggregates. This stage occurs in three stages: first, exsolution in the magnetite-ulvöspinel-spinel system (separation of Zn-Cr-hercynite, 800–1000 °C); later, in the magnetite-ulvöspinel system (separation of ulvöspinel, about 500 °C); and finally oxidizing exsolution with the genesis of ilmenite (590–410 °C with $-\log fO_2$ being 21 and 33, respectively).

Evolutionary features of mineral assemblages suggest that hortonolitic dunites underwent, partly at least, a magmatic stage and a lengthy stage of subsolidus autometamorphic transformations under the influence of metal-bearing fluid.

Low solubility of platinoids in silicate and low-sulfur sulfide melts probably was the reason for, on the one hand, direct crystallization of PGM from melt, unrelated to separations of primary sulfide phase, and, on the other hand, concentration of platinum group elements (PGE) in fluid. The PGE-rich fluid generated numerous PGM assemblages both at the stage of crystallization of residual melt which concentrated iron and titanium (inclusions in titanomagnetite) and as the result of intense medium-temperature autometasomatic reworking of primary hortonolitic dunites (simultaneously with minerals of the late chlorite-magnetite-amphibole assemblage).

Zusammenfassung

Entwicklung der Platin-Mineralisation in den Horthonolit-Duniten der Mooihoek und Onverwacht Pipes, Bushveld-Komplex

Minerale der Platingruppe (PGM) und assoziierte Silikate, Oxide und Sulfide aus vier Proben von Platin-führenden Hortonolith-Duniten der Mooihoek und Onverwacht-Pipes, Bushveld-Komplex, führen die folgenden Mineralassoziationen: 1. (Pt, Fe) Legierung, die in ihrer Zusammensetzung Isoferroplatin ähnlich und syngenetisch mit Olivin ist 2) Sperrylith, der syngenetisch mit Klinopyroxen ist 3) Tetraferroplatin, Laurit, Hollingworthit, ein noch nicht benanntes Mineral (Rh, Ru) AsS, das syngenetisch mit Titanomagnetit ist 4) Tetraferroplatin (?), Sperrylith, Geversit, Hollingworthit, Platarsit, Cabriit, Rustenburgit, Sobolevskit (?) sowie die noch nicht benannten Minerale $(Pd, Pt)_4(Cu, Fe)_2(Sn, Sb)_3$, $(Pt, Ir)_3Sb$, (Rh, Ir, Pt)SbS, Rh(Sb, Bi)S, and Pt(Bi, Sb), die syngenetisch mit späten Amphibolen, Magnetit, Chlorit, Ilmenit und Pentlandit sind.

Feine (weniger als 0.1 mm) tröpfchenförmige Sulfideinschlüsse, die aus Troilit, eisenreichem Chalcopyrit und eisenreichem Pentlandit bestehen und von winzigen Körnern von Magnetit, Ilmenit, Amphibol und Biotit umgeben sind, kommen im Olivin vor. Die Gesamtzusammensetzung dieser Einschlüsse ist bei niedriger Schwefelfugazität im Gleichgewicht mit einer eisenreichen Silikatschmelze.

Die Temperaturen, bei denen die verschiedenen Mineralgesellschaften gebildet wurden, wurden in einer Probe von Titanomagnetit-reichem Wehrlit untersucht, und die folgenden Stadien wurden identifiziert: 1) ein Hochtemperaturstadium (980–1020 °C), das auf der Basis von Zwei-Pyroxen-Thermometrie bestimmt wurde und 2) ein Hoch- bis Mitteltemperaturstadium, das auf der Basis von Entmischungstexturen von Titanomagnetit-Aggregaten gemessen wurde. Hier sind drei Gruppen zu unterscheiden:

1.) Entmischung im Magnetit-Ulvöspinell-Spinell-System (Bildung von Zn-Cr-Hercynit, 800–1000 °C); später, im Magnetit-Ulvöspinell-System (Abtrennung von Ulvöspinell bei ungefähr 500 °C) und schließlich oxidierende Entmischung mit Entstehung von Ilmenit (590–410 °C mit-log fO2 von 21 bzw. 33).

Die beobachteten Mineralvergesellschaftungen weisen darauf hin, daß die Horthonolit-Dunite zumindest teilweise ein magmatisches Stadium durchlaufen haben und daß sich dann ein sehr ausgedehntes Stadium von autometamorphem Subsolidusumwandlungen unter dem Einfluß von metallführenden Fluiden anschloß.

Die niedrige Löslichkeit von Platinmetallen in Silikatschmelzen und in schwefelarmen Sulfid-Schmelzen war wahrscheinlich der Grund dafür, daß einerseits eine direkte Kristallisation von PGM aus der Schmelze erfolgte, die in keinerlei Beziehung zur Abtrennung einer primären Sulfidphase stand und daß andererseits Konzentrationen der Platingruppenelemte (PGE) in Fluiden zustande gekommen sind. Die PGE-reichen Fluide führten zur Entstehung zahlreicher PGM-Vergesellschaftungen und zwar sowohl im Stadium der Kristallisation der Restschmelze, die Eisen- und Titan konzentrierte (Einschlüsse in Titanmagnetit) und als Resultat intensiver auto-

metasomatischer Beeinflussung bei mittleren Temperaturen der primären Horthonolit-Dunite gleichzeitig mit den Mineralen der späten Fluid-Magnetit-Amphibol-Vergesellschaftung.

Introduction

An extensive literature exists on the geology, petrography, and mineralogy of the Onverwacht, Mooihoek, and Driekop platiniferous dunite pipes of the eastern Bushveld Complex. The "pipe-like" type of deposits played an important part in production of platinum-group elements (PGE's) right up to 1961. *Wagner* (1929) gave a comparative review of the geology and petrography of the bodies, and the PGE mineralogy was studied in detail by *Stumpfl* (1961, 1962); *Stumpfl* and *Clark* (1965); *Cabri* et al. (1977a, b), among others. It was noted that Pt-Fe alloys, Pt, Ir, and Rh arsenide and sulfarsenide, and combinations of Sb and Bi platinoids make up the major portion of the PGM assemblage. It was determined that PGM assemblages of the pipes are distinct from those of the Merensky Reef, which are dominated by Pt and Pd sulfide (braggite, vysotskite), and locally Pt and Pd tellurides (moncheite, merenskyite, kotulskite, michenerite). At the same time, *Peyerl* (1982) showed that the PGM assemblage of the Merensky Reef markedly approximates that of "pipe-like" deposits in the vicinity of dunite pipes. Thus, processes of mineral genesis, or of PGM genesis at least, of both types of ores of the Bushveld complex are probably genetically interrelated.

In spite of a long history of investigation and highly detailed studies, the nature of formation of dunite pipes and their associated PGE mineralization is still a point of controversy. Two alternative hypotheses are discussed: 1) a magmatic origin of dunite pipes, *Wagner* (1929); *Naldrett* and *Cabri* (1976); *Naldrett* and *Duke* (1980), among others; 2) an origin of dunite pipes as the result of metasomatic processes (*Cameron* and *Desborough* (1964); *von Gruenewaldt* (1979), *Stumpfl* and *Rucklidge* (1982), *Schiffries* (1982), among others). This problem remains a current question in the attempt to understand the petrology of layered mafic-ultramafic intrusions as a whole and the genesis of associated PGE deposits. In analysis of works published on the problem one could not but note that, as a rule, either pipes proper—their geology, petrography, geochemistry, mineralogy of pipe-forming rocks, or their PGE mineralization proper were investigated. The present authors believe that new types of genetic information, including that on the origin of dunite pipes as a whole, can be obtained by reconstructing paragenetic processes of evolution of all the constituents of the bodies, both rock-forming minerals (primary and secondary) and assemblages of associated accessories, especially the PGM.

Subjects and Methods of Investigation

In 1929, the Soviet geologist *M. I. Lipovsky* collected samples of platiniferous rocks and ores from working mines in the Bushveld Complex; collection No. 2480 was taken to the Central Geological Exploration Museum (TsNIGR), All-Union Geological Institute (VSEGEI), St. Petersburg, USSR. An opportunity to examine this collection was given to the authors. In examining the samples with an optical microscope, the authors picked out four polished sections of hortonolitic dunites from the Mooihoek and Onverwacht pipes in which the main PGM assemblages which formed at different times were represented: 1) sample 19—hortonolitic dunite

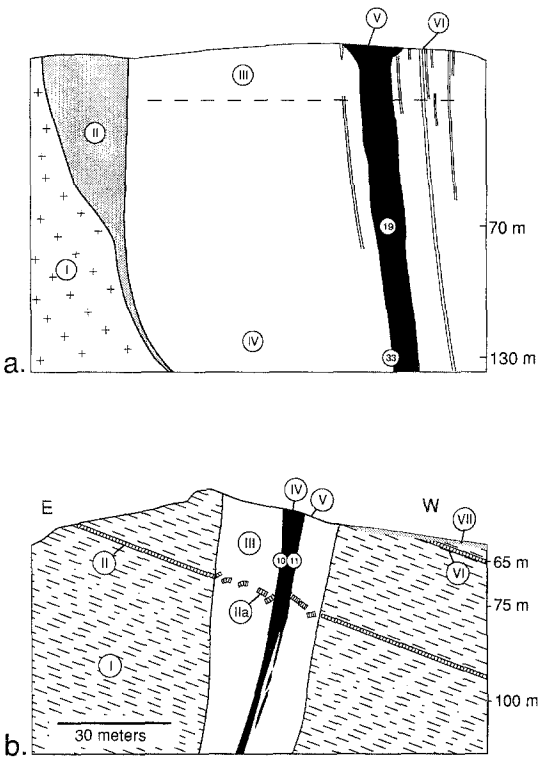

Fig. 1. Diagrammatic sections of the Mooihoek and Onverwacht pipes, Bushveld Complex (after Wagner, 1929) showing the position of samples of hortonolite dunites (19, 33, 10, 11). a) Mooihoek pipe: I anorthosite leuconorite; II coarse-grained diallagite, feldspathic pyroxenite, and olivine-norite; III serpentine and silicified serpentine replacing dunite; IV serpentinized dunite (wehrlite); V pipe of hortonolitic dunite; VI veins of pegmatoid hortonolitic dunite and wehrlite, hornblende-pyroxene-phlogopite and phlogopite-pyroxene-hornblende-magnetitic rocks. b) Onverwacht pipe: I bronzitite containing disseminated chromite; II lower chromite horizon; IIa xenoliths of chromitite in dunite; III dunite and wehrlite; IV main body and veins of hortonolite dunite; V veins of pyroxene-hornblende-hortonolitic rock; VI upper chromite horizon; VII platinum-bearing debris and eluvium

with Pt content being 7.5 g/t, Mooihoek, horizon 70 m; 2) sample 33—dunite poor in Pt at the boundary with dunite rich in Pt, Mooihoek, horizon 130 m; 3) sample 11—PGE-rich dunite, Onverwacht, horizon 65 m; 4) sample 10—separation of titanomagnetite in the rocks associated with the same horizon. (The authors have retained the sample numbering scheme of *M. I. Lipovsky*.) Figure 1 shows the position of the samples studied in diagrammatic sections of the pipes (*Wagner*, 1929).

Polished sections were thoroughly examined with an optical microscope which allowed determination of textural relationships of PGM assemblages, associated rock-forming silicates, oxides and sulfides. The minerals were subsequently examined under a Camscan electron microscope-microanalyzer equipped with a Link-10000 energy dispersive system at the Center of Physico-Chemical Studies of Material, Mekhanobr Institute, St. Petersburg.

Results

Assemblages of Silicates and Oxides

All the samples studied are typical hortonolitic dunites. They (except sample 10) are dominated by olivine which contains 46.0–49.7 mol.% Fo (Table 1, analyses 1, 2, 7, 21). Pyroxenes and titanomagnetite, xenomorphic with respect to olivine, also represent primary minerals of the rocks (samples 10, 11). In sample 10, concentrations of titanomagnetite are responsible for the sideronitic texture of this hortonolitic wehrlite (Fig. 2a). At strong magnification, pyroxene grains show exsolution textures with the matrix being clinopyroxene (Table 1, analysis 22) and the lamellae being orthopyroxene (Table 1, analysis 23).

Table 1. *Microprobe compositions of silicates and oxides from the Mooihoek and Onverwacht hortonalitic pipes of the Bushveld Complex*

Number	1	2	3	4	5	6	7	8	9	10	11	12	13	14	15	16
Sample	11	19	19/3.1	19/3.1	19/3.1	19/3.1	19/3.2	19/3.2	19/3.2	19/13	19/15	19/3.3	19/3.3	19/12	19/12	19/12
Mineral	Ol	Ol	Bt	Hb	Ilm	Mt	Ol	AmfR	Ilm	Mt	Cpx	Act	Mt	Hb	Act	Chl
SiO2	34.8	35.0	36.7	46.0	0.2	0.3	35.0	56.0	0.2	0.2	53.3	56.3	-	42.6	57.8	33.9
TiO2	-	-	0.9	0.5	50.2	0.4	-	0.4	50.1	0.6	-	-	0.5	1.8	-	0.2
Al2O3	-	-	16.5	7.6	-	0.1	-	0.5	-	-	-	1.8	-	10.7	-	12.1
Cr2O3	-	-	0.2	-	-	-	-	-	-	0.9	-	-	-	-	-	-
V2O3	-	-	-	-	0.7	0.5	-	-	0.6	1.2	-	-	-	-	-	-
Fe2O3	-	-	-	9.1	1.6	67.9	-	-	1.6	62.2	-	-	68.0	4.6	-	-
FeO	42.4	42.9	12.8	4.1	45.6	30.8	41.8	18.9	45.7	31.1	6.3	7.4	30.9	10.2	4.7	10.6
MnO	0.8	-	-	-	0.8	-	-	1.1	1.1	-	-	-	0.6	-	-	-
MgO	22.0	22.0	19.1	16.1	0.7	0.2	23.2	20.6	0.6	-	16.4	19.5	-	13.1	22.2	30.8
CaO	-	0.2	-	10.9	-	-	-	0.6	-	-	23.9	12.4	-	11.5	12.8	-
Na2O	-	-	1.4	3.1	-	-	-	-	-	-	-	-	-	3.5	-	-
K2O	-	-	7.9	0.2	-	-	-	-	-	-	-	0.2	-	0.1	-	-
NiO	-	-	-	0.3	-	-	-	-	-	-	-	-	-	-	-	-
ZnO		-	-	-	-	-	-	-	-	-	-	-	-	-	-	-
Cl	-	-	-	0.2	-	-	-	-	-	-	-	-	-	0.2	-	0.2
Total	100.0	100.1	95.9	98.0	99.8	100.2	100.0	98.1	99.9	96.2	99.9	97.6	100.0	98.2	97.5	87.7

Number	17	18	19	20	21	22	23	24	25	26	27	28	29	30	31	32	33
Sample	19/12	19/7	19/4	19/14	10	10	10	10/1	10/1	10/1	10/1	10/1	10.1	10/8	10/2H	10/13	10/13
Mineral	Mt	Mt	Act	Mt	Ol	Cpx	Opx	TiMt	TiMt	Hz	Hz	Ulv	Ilm	Ilm	Mt	Hz	Ilm
SiO2	0.5	-	57.2	-	33.6	50.5	49.1	0.2	0.2	0.2	0.5	0.2	-	-	0.2	0.2	0.2
TiO2	0.2	3.7	-	0.6	-	0.8	0.3	7.6	9.9	7.4	1.1	32.1	52.2	51.9	1.6	0.7	51.1
Al2O3	-	-	-	-	-	1.5	0.7	0.9	3.6	45.2	55.9	1.7	-	-	-	60.4	0.4
Cr2O3	-	1.9	-	-	0.2	-	-	1.2	2.9	1.7	5.4	-	-	-	-	1.5	-
V2O3	-	-	-	-	-	-	-	1.3	1.3	0.9	-	-	0.5	0.4	0.2	0.2	0.3
Fe2O3	67.4	59.3	-	67.8	-	-	-	48.1	38.7	-	-	-	-	-	65.2	-	-
FeO	31.5	34.6	5.7	31.6	44.3	11.3	26.4	40.2	41.4	32.7	23.1	61.6	44.2	44.7	32.3	21.2	45.5
MnO	0.4	-	0.6	-	0.6	0.3	0.4	0.3	0.4	0.3	-	0.6	0.5	0.7	-	-	0.7
MgO	-	0.5	21.0	-	21.2	13.1	16.6	0.2	0.8	9.6	10.6	1.1	2.4	2.0	0.5	11.3	1.5
CaO	-	-	12.6	-	-	21.8	5.6+	-	-	-	-	-	-	-	-	-	-
Na2O	-	-	0.5	-	-	-	-	-	-	-	-	-	-	-	-	-	-
K2O	-	-	-	-	-	-	-	-	-	-	-	-	-	-	-	-	-
NiO	-	-	-	-	-	-	-	-	-	-	0.3	0.3	-	-	-	-	-
ZnO	-	-	-	-	-	-	-	-	0.7	2.0	3.0	-	-	-	-	4.3	-
Cl	-	-	-	-	-	-	-	-	-	-	-	-	-	-	-	-	-
Total	100.0	100.0	97.6	100.0	99.9	99.3	99.1	100.0	99.4	100.0	99.9	97.6	99.8	99.7	100.0	99.8	99.7

Ol-olivine, Bt-biotite, Hb-hornblende, Ilm-ilmenite, Mt-magnetite, AmfR-rhombic amphibole(?), Cpx-clinopyroxene, Act-actinolite, Chl-chlorite, Opx-orthopyroxene, TiMt-titanomagnetite, Hz-hercynite, Ulv-ulvöspinel; FeO and Fe_2O_3 calculated on the mean of ideal crystallochemistry of minerals; *Total sum including O=Cl; +influence of Cpx matrix. Standards: Na, Mg, Al, Si—jadeite; K—sanidine; Ca, Ti—wollastonite; Cl—sodalite; V, Mn, Fe, Cr, Ni, Zn—pure metals.

Titanomagnetite occurs as a complex polymineralic aggregate with a multistage exsolution texture. Large lamellae (up to 0.05 mm in thickness) of ilmenite occur in a matrix of titanomagnetite (Fig. 2b; Table 1, analyses 29, 30). Boundaries of ilmenite lamellae are marked by continuous chains of fine (1–5 μm) grains of Cr-Zn-hercynite (Table 1, analysis 27). Three oriented systems of fine (1–3 μm and under) ingrowths of the same spinellid (Table 1, analysis 26) and lamellae of ulvöspinel (Table 1, analysis 28) were also observed in titanomagnetite. Separations of ulvöspinel are usually bordered by microgrowths of Cr-Zn hercynite. Narrow (5–7 μm) zones free of ingrowths always occur near lamellae of ilmenite in titanomagnetite (Fig. 2b). As a rule, the titanomagnetite of these zones (Table 1, analysis 25) is rich in trace elements (Al, Ti, Cr, Mg, Zn), as compared to matrix-titanomagnetite (Table 1, analysis 24). It should be noted that hercynite and ulvöspinel rich in different trace elements were not encountered previously, even in detailed microprobing of spinellid

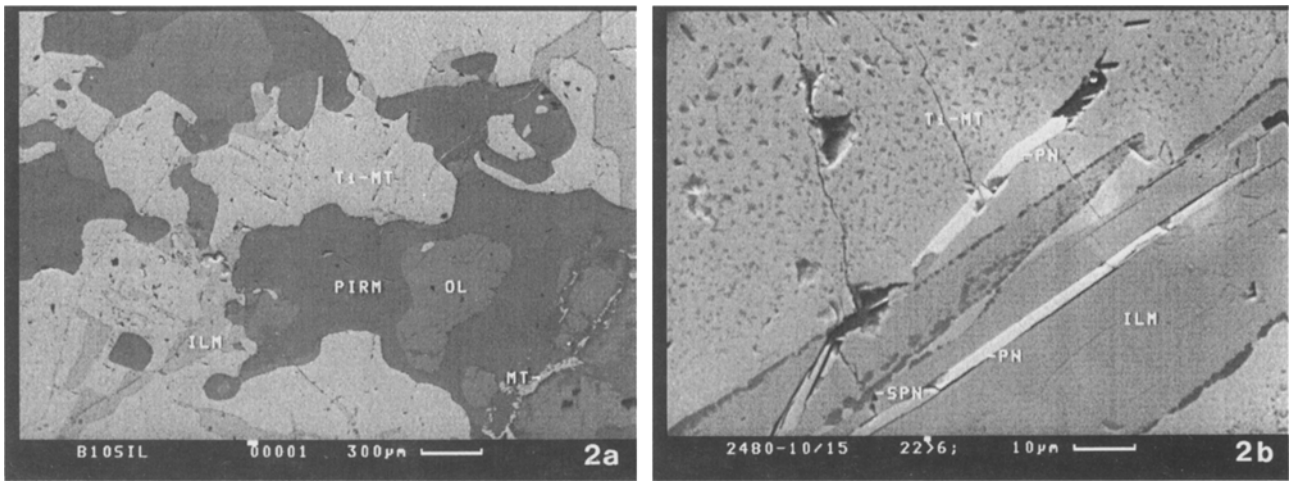

Fig. 2. Textural relations of minerals in titanomagnetite-rich wehrlite from hortonolitic dunites, sample 10. Scanning electron microscope (SEM) photographs are shown here and in Figs. 3 through 9. a) rock texture: OL olivine, PIRM clinopyroxene, TI-MT titanomagnetite, ILM ilmenite, MT magnetite, b) exsolution texture of titanomagnetite (sample 10): SPN, Cr-Zn-hercynite; PN, cobalt-pentlandite

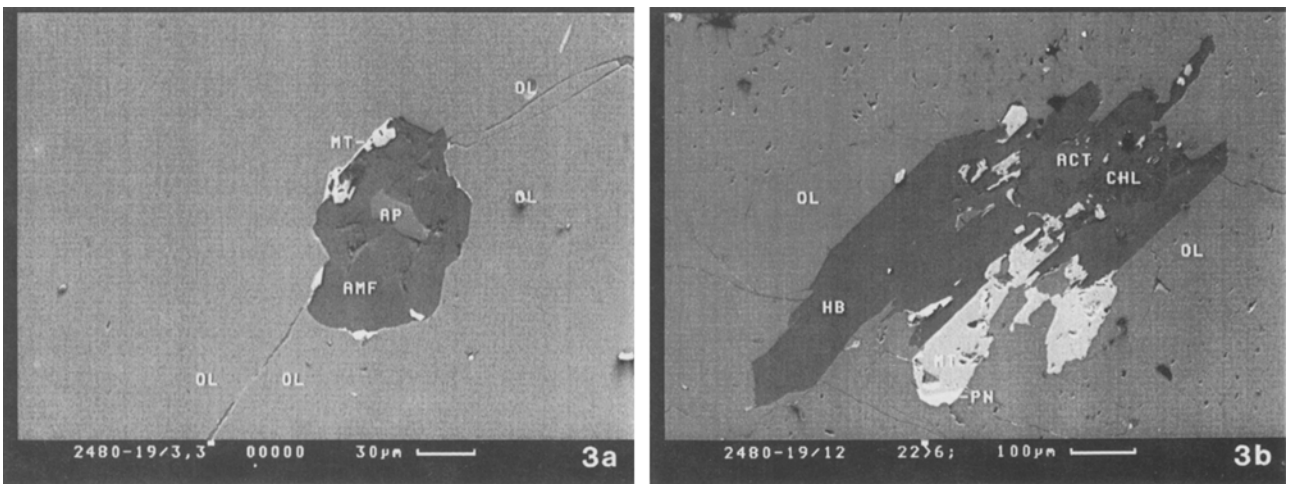

Fig. 3. Development of late chlorite-magnetite-amphibole assemblage (sample 19) along the grain boundaries (a, sample 19/3.3) or in joints of olivine crystals (b, sample 19/12). HB hornblende, ACT and AMF actinolite, CHL chlorite, PN pentlandite, AP apatite

assemblages of different rocks from the dunite pipes of the Bushveld Complex (*Stumpfl* and *Rucklidge*, 1982).

Later-formed minerals such as amphiboles, magnetite, chlorite, and locally ilmenite and pentlandite are common along olivine grain boundaries (Fig. 3a) and along crossing joints (Fig. 3b). Rare crystals of apatite are also associated with these minerals (Fig. 3b). Amphiboles occur as aggregates, composed of columnar, prismatic, and needle-shaped grains with intergranular pores filled, as a rule,

with magnetite or chlorite and magnetite. In this assemblage, magnetite also forms monomineralic streaky concentrations which replace olivine.

Amphiboles are pargasitic hornblende (Table 1, analysis 14) or actinolite (Table 1, analyses 12, 15) which can form joint aggregates. High TiO_2 (1.8 wt.%), some K_2O, and the presence of Cl (0.2 wt.%) are typical. Accessory apatite, associated with actinolite and magnetite, is rich in chlorine (2.9 wt.% Cl; sample 19/3.3). Chlorite here (Table 1, analysis 16) occurs as clinochlore and also contains chlorine (0.2 wt% Cl). Magnetite as monomineralic and as magnetite-amphibole aggregates contains only low concentrations of TiO_2 and MnO (Table 1, analyses 13, 17). If ilmenite appears in the assemblage, magnetite becomes TiO_2-rich and contains some Cr_2O_3 (Table 1, analysis 18).

Sulfide Assemblages

Rocks of dunite pipes are relatively poor in Fe, Ni, and Cu sulfides (*Stumpfl* and *Rucklidge*, 1982). Taking into account the significance on the PGE distribution of a possible presence of even low amounts of sulfide melt in the formation of platiniferous dunite pipes, let us discuss the different assemblages of the sulfides of chalcophile metals in the samples studied. The abundances of these minerals is extremely low (about 0.1 vol.%). At the same time, relationships between sulfides and enclosing silicates and oxides suggest that assemblages of sulfide formed at different times in the pipe dunites.

Fine (0.1 mm and under) drop-shaped and spherical aggregates (microglobules) of Fe, Cu, and Ni sulfides, occurring as inclusions in the central parts of nonbroken grains of olivine, were identified in sample 19 (Fig. 4). The inclusions generally consist of troilite and chalcopyrite or of troilite, chalcopyrite, and pentlandite. The primary character of these inclusions is supported by minute grains of olivine found in them (Fo_{49}; Table 1, analysis 7). It should be emphasized that such "microdrops" of sulfide are usually accompanied by micrograins of ilmenite and magnetite, as well as silicates containing alkaline and volatile components—biotite, hornblende, or rhombic amphibole (?), localized along the periphery of microdrops (Fig. 4; Table 1, analyses 3, 4, 5, 6, 8, 9).

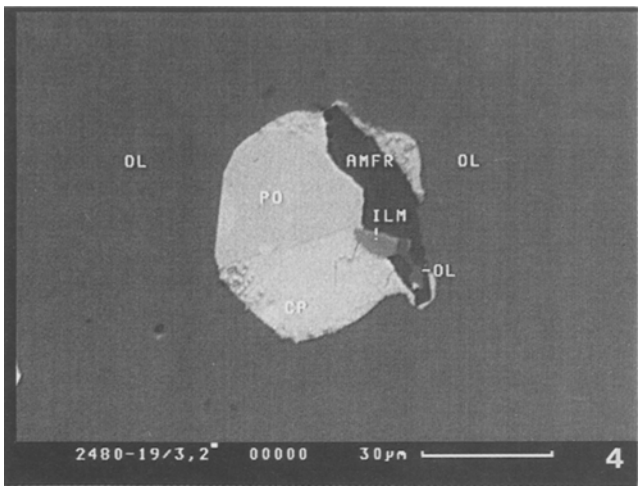

Fig. 4. Sulfide globule included in the central part of a non-broken grain of olivine, sample 19, area 3.2). OL olivine, PO troilite, CP chalcopyrite, AMFR rhombic amphibole(?), ILM ilmenite

Table 2. *Composition of Sulfides in Hortonolite Dunite of the Mooihoek and Onverwacht Dunite Pipes, Bushveld Complex*

Analysis	1	2	3	4	5	6	7	8	9	10	11	12	13	14	15	16
Sample	19/3.1	19/3.1	19/3.2	19/3.2	19.8	19.8	19.8	19/6.2	19.12	19/15	10.8	10.8	10.8	10/2H	10/13	10/15
Mineral	Tr	Cp	Tr	Cp	Tr	Cp	Pn	Pn	Pn	Sl	Pn	Cp	Cub	Co-Pn	Co-Pn	Co-Pn
wt. %																
Fe	63.3	34.4	63.1	35.2	63.3	35.3	38.0	33.6	31.4	8.3	44.8	32.6	41.6	15.9	23.8	24.5
Ni	-	0.4	-	0.4	-	0.3	23.8	24.6	28.4	-	16.6	-	-	14.0	18.8	15.4
Cu	0.2	29.7	-	29.0	-	29.2	-	-	-	-	-	34.2	23.5	-	-	-
Co	-	-	-	-	-	-	5.1	8.7	7.3	-	6.0	-	-	39.5	23.6	27.7
Zn	-	-	-	-	-	-	-	-	-	57.3	-	-	-	-	-	-
Cd	-	-	-	-	-	-	-	-	-	0.1	-	-	-	-	-	-
S	36.4	35.2	36.4	35.0	36.4	35.2	32.8	33.1	33.0	34.0	32.1	33.0	34.2	30.1	33.4	32.1
Sum	99.9	99.7	99.5	99.6	99.7	100.0	99.7	100.0	100.1	99.7	99.5	99.8	99.3	99.5	99.6	99.7
atomic ratio																
Fe	1.00	1.13	0.99	1.15	1.00	1.15	5.27	4.64	4.36	0.14	6.24	1.09	2.05	2.27	3.31	3.43
Ni	-	0.01	-	0.01	-	0.01	3.14	3.24	3.70	-	2.19	-	-	1.90	2.48	2.06
Cu	-	0.85	-	0.84	-	0.84	-	-	-	-	-	1.00	1.02	-	-	-
Co	-	-	-	-	-	-	0.67	1.15	0.96	-	0.79	-	-	5.34	3.11	3.67
Zn	-	-	-	-	-	-	-	-	-	0.84	-	-	-	-	-	-
S	1.00	2.01	1.01	2.00	1.00	2.00	7.92	7.97	7.98	1.02	7.78	1.91	2.93	7.48	8.09	7.84

Standards: S—pyrite; all others—pure elements

Of the trace elements, only copper in troilite (up to 0.2 wt.%) was determined (Table 2, analyses 1, 3, 5). Chalcopyrite (Table 2, analyses 2, 4, 6) is nonstoichiometric: the atomic Fe/Cu ratio is 1.33–1.37 and corresponds to the composition of its iron-rich variety (Karpenkov et al., 1974). Like iron-rich chalcopyrite of the Noril'sk deposits, it is always characterized by the presence of Ni (0.3–0.4 wt%). Pentlandite of the "microdrops" is also rich in iron, (Fe/Ni = 1.43 at.%), and contains considerable Co (5.1 wt%; Table 2, analysis 7).

A late generation of pentlandite in the sample is represented by streaky separations, localized along the grain boundaries of olivine and in magnetite-amphibole aggregates (Fig. 3b; Table 2, analysis 9). The pentlandite is richer in nickel (Fe/Ni = 1.18) and rich in Co (7.3 wt.%) as compared to pentlandite of the "microdrops" of sulfide in olivine.

Two other generations of sulfide were recognized in segregations of titanomagnetite in hortonolitic dunites (sample 10). The first generation is represented by fine (less than 50 μm) microglobules, rich in copper, included in ilmenite (Table 1, analysis 30). The microglobules are made up of chalcopyrite, cubanite, and pentlandite. The compositions of chalcopyrite (Table 2, analysis 12) and cubanite (Table 2, analysis 13) differ slightly from the stoichiometric composition. Pentlandite (Table 2, analysis 11) is rich in iron, with an Fe/Ni ratio of 2.85 at.%, and contains 6.0 wt% Co.

Streaky sulfide separations, localized along the boundaries of ilmenite lamellae with surrounding titanomagnetite, are later forms relative to ilmenite lamellae (and sulfide xenocrysts in them) (Fig. 2b). This extremely cobalt-rich sulfide (27.7 wt.%), can be considered as cobalt-pentlandite (Table 2, analysis 16).

Platinum-Group Mineral Assemblages

PGM were identified in all the main assemblages of rock-forming minerals of hortonolitic dunites. Monomineralic inclusions of Pt-Fe alloys are the earliest-formed segregations of PGM in the rocks; the inclusions were found in the central

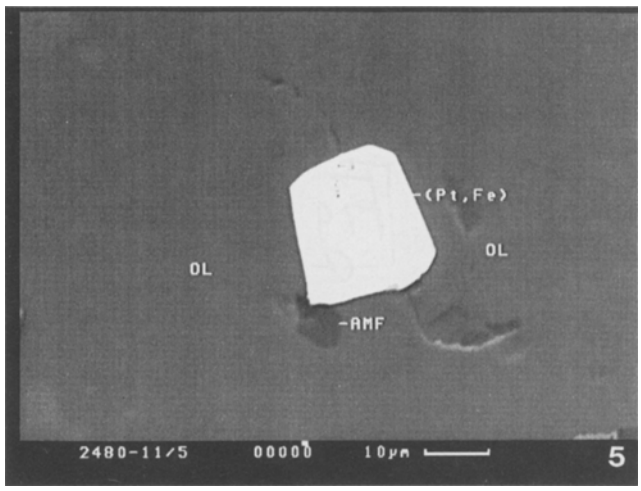

Fig. 5. Microinclusion of (Pt, Fe) alloy in the central part of a crack-free olivine grain. Sample 11, site 5

parts of nonbroken grains of olivine (samples 11 and 19). They are represented by either drop-shaped forms or by idiomorphic crystals (Fig. 5). Micrograins of magnetite (Table 1, analysis 18) and rhombic amphibole (?) are localized along the boundaries of the inclusions. Pt-Fe alloy (Table 3, analyses 1, 2) lies in the stability field of iron-rich platinum or isoferroplatinum with the composition 30–33 at.% Fe (*Cabri* and *Feather*, 1981). Precise identification of the minerals requires X-ray diffraction analysis.

Segregations of sperrylite ($PtAs_2$) occurring as chains of "microdrops" may have been formed in interstices of olivine grains (Fig. 6a) simultaneously with clinopyroxene in hortonolitic dunites (sample 19). Evidence for this is the occurrence of fine (1–5 μm and under) drop-shaped ingrowths of clinopyroxene (Fig. 6b; Table 1, analysis 11) in sperrylite (Table 3, analysis 3). Micrograins of rhombic amphibole (?) and sphalerite (Table 2, analysis 10) are localized along the boundaries of the segregations.

PGM are also present in titanomagnetite of hortonolitic dunites (sample 10). Inclusions of crystals of a Pt-Fe mineral (Table 3, analyses 25, 28) intergrown with either laurite (RuS_2, Table 3, analysis 26) and hollingworthite ((Rh, Ru, Pt, Ir)AsS, Table 3, analysis 27), or with magnetite (Table 1, analysis 31) and cobalt-pentlandite (Table 2, analysis 14) were found in large lamellae of ilmenite (Fig. 7). A PGM aggregate, composed of the same Pt-Fe mineral (Table 3, analysis 29), an unnamed mineral ((Rh, Ru)(Ni, Fe)(AsS), Table 3, analysis 30), and orcelite containing admixtures of Ru and Pt ($(Ni, Fe, Co)_2(As, S)$, Table 3, analysis 31), was found directly in titanomagnetite. The aggregate is bordered by zones of cobalt-pentlandite (Table 2, analysis 15), Cr-Zn-hercynite (Table 1, analysis 32), and ilmenite (Table 1, analysis 33) which replace each other in succession. Unlike Pt-Fe alloy enclosed in olivine (Table 3, analyses 1, 2), this Pt-Fe mineral (Table 3, analysis 32) is poor in PGEs and has a higher proportion of Fe, Cu and Ni. In composition (ΣFe + Ni + Cu 46–49 at.%), the mineral conforms to tetraferroplatinum Pt(Fe, Cu, Ni) (*Cabri* and *Feather*, 1981; *Bowles*, 1990); however, this tentative identification requires X-ray diffraction support.

The most numerous finds and types of PGM assemblages in the samples studied are related to occurrences of late minerals such as amphiboles, chlorite, magnetite,

Table 3. *Microprobe Analyses of Platinum-Group Minerals from the Mooihoek and Onverwacht Hortonolite Pipes of the Bushveld Complex*

1	Pt-Fe Alloy	$(Pt_{0.60}Fe_{0.30}Pd_{0.05}Rh_{0.05})_{1.00}$
2	Pt-Fe Alloy	$(Pt_{0.61}Fe_{0.33}Rh_{0.02}Ni_{0.02}Pd_{0.01}Cu_{0.01})_{1.00}$
3	Sperrylite	$(Pt_{0.97}Fe_{0.03}Rh_{0.01})_{1.01}(As_{1.97}S_{0.03})_{2.00}$
4	Hollingworthite	$(Pt_{0.47}Ru_{0.26}Pt_{0.21}Fe_{0.10}Ni_{0.02}Ir_{0.01})_{1.07}As_{0.86}S_{1.07}$
5	Tetraferroplatinum(?)	$Pt_{0.98}(Fe_{0.82}Ni_{0.12}Cu_{0.08})_{1.02}$
6	Tetraferroplatinum(?)	$Pt_{1.01}(Fe_{0.66}Cu_{0.20}Ni_{0.13})_{0.99}$
7	Cabriite	$(Pd_{1.60}Pt_{0.30})_{1.90}(Cu_{0.84}Fe_{0.23})_{1.07}(Sn_{0.55}Sb_{0.47})_{1.02}$
8	Cu-Rustenburgite	$(Pt_{1.17}Pd_{0.54}Cu_{0.90}Fe_{0.36})_{2.97}Sn_{1.03}$
9	Unknown	$(Pd_{2.99}Pt_{1.08})_{4.07}(Cu_{1.82}Fe_{0.16})_{1.98}(Sn_{2.82}Sb_{0.13})_{2.95}$
10	Pt-Fe Alloy	$(Pt_{0.68}Fe_{0.30}Ni_{0.01})_{0.99}$
11	Tetraferroplatinum(?)	$Pt_{1.04}(Fe_{0.61}Cu_{0.35})_{0.96}$
12	Bi-Geversite	$Pt_{1.00}(Sb_{1.66}Bi_{0.29}As_{0.04})_{1.99}$
13	Hollingworthite	$(Rh_{0.54}Pt_{0.20}Ir_{0.20}Fe_{0.02})_{0.96}(As_{1.00}Sb_{0.03})_{1.03}S_{1.00}$
14	Platarsite	$(Pt_{0.37}Ir_{0.34}Rh_{0.26}Fe_{0.07})_{1.04}(As_{1.08}Sb_{0.02})_{1.10}S_{0.86}$
15	Sperrylite	$(Pt_{1.00}Ir_{0.08})_{1.08}(As_{1.65}S_{0.18}Sb_{0.09})_{1.92}$
16	Unknown	$(Pt_{2.43}Ir_{0.36}Fe_{0.18}Cu_{0.07})_{3.04}Sb_{0.96}$
17	Pt-Fe Alloy	$(Pt_{0.69}Fe_{0.30}Ni_{0.01})_{1.00}$
18	Tetraferroplatinum(?)	$Pt_{1.05}(Fe_{0.73}Cu_{0.13}Ni_{0.09})_{0.95}$
19	Hollingworthite	$(Rh_{0.87}Fe_{0.05}Pt_{0.06}Ir_{0.04}Ru_{0.02})_{1.04}(As_{0.96}Sb_{0.01})_{0.97}S_{0.99}$
20	Unknown	$(Rh_{0.79}Pt_{0.11}Ir_{0.09}Fe_{0.08}Co_{0.01})_{1.08}(Sb_{0.91}As_{0.04}Bi_{0.04}Sn_{0.02})_{1.01}S_{0.91}$
21	Unknown	$(Rh_{0.93}Fe_{0.12}Ir_{0.03}Pt_{0.02})_{1.10}(Sb_{0.65}Bi_{0.32}Sn_{0.02}As_{0.02})_{1.01}S_{0.90}$
22	Pt-Sb-Sobolevskite(?)	$(Pd_{0.67}Pt_{0.29}Fe_{0.11})_{1.07}(Bi_{0.70}Sb_{0.23})_{0.93}$
23	Unknown	$(Pt_{0.72}Fe_{0.21}Cu_{0.02})_{0.95}(Bi_{0.85}Sb_{0.19})_{1.04}$
24	Ru-Pentlandite	$(Fe_{4.23}Ni_{3.24}Co_{0.96}Ru_{0.60}Rh_{0.07})_{9.10}S_{7.90}$
25	Tetraferroplatinum(?)	$(Pt_{1.06}Rh_{0.01})_{1.07}(Fe_{0.65}Cu_{0.17}Ni_{0.10})_{0.92}$
26	Laurite	$(Ru_{0.90}Pt_{0.04}Os_{0.02}Fe_{0.02}Rh_{0.01})_{0.99}(S_{1.99}As_{0.02})_{2.01}$
27	Hollingworthite	$(Rh_{0.38}Ru_{0.20}Pt_{0.17}Ir_{0.16}Fe_{0.06}Os_{0.03})_{1.00}As_{0.73}S_{1.26}$
28	Tetraferroplatinum(?)	$(Pt_{1.02}Ir_{0.02})_{1.04}(Fe_{0.73}Cu_{0.11}Ni_{0.11})_{0.95}$
29	Tetraferroplatinum(?)	$(Pt_{1.01}Rh_{0.01})_{1.02}(Fe_{0.78}Cu_{0.10}Ni_{0.10})_{0.98}$
30	Unknown	$(Rh_{0.83}Ru_{0.07})_{0.90}(Ni_{0.90}Fe_{0.18}Co_{0.06})_{1.14}(As_{0.81}S_{0.15})_{0.96}$
31	Fe-Co-Orcelite	$(Ni_{1.61}Fe_{0.20}Co_{0.11}Ru_{0.04}Cu_{0.02}Pt_{0.01})_{1.99}(As_{0.65}S_{0.35})_{1.00}$

Standards: S–pyrite; As–IAs; all others–pure metals

Number	1	2	3	4	5	6	7	8	9	10	11	12	13	14	15	16
Sample	19/2	19/13	19/15	19/6.2	19/6.1	19/14	19/14	19/14	19/4	11/1	11/1	11/1	11/1	11/1	11/1	11/1
Pt	80.6	84.0	55.7	18.1	76.6	77.6	13.8	46.7	21.0	87.4	78.3	41.8	16.9	26.0	54.2	70.3
Pd	3.8	0.9	-	-	-	-	40.3	11.9	31.7	-	-	-	-	-	-	-
Rh	3.6	1.6	0.3	21.5	-	-	-	-	-	-	-	-	22.5	9.5	-	-
Ru	-	-	-	1.2	-	-	-	-	-	0.5	-	-	15.4	23.1	4.5	10.2
Ir	-	-	-	11.8	-	-	-	-	-	-	-	-	-	-	-	-
Os	-	-	-	-	-	-	-	-	-	-	-	-	-	-	-	-
Fe	11.4	13.2	0.4	2.5	18.6	14.5	3.0	4.1	0.9	11.2	13.8	-	0.5	1.5	-	1.5
Cu	-	0.6	-	-	2.1	4.9	12.6	11.8	11.5	-	8.6	-	-	-	-	0.6
Ni	-	0.7	-	0.6	2.8	3.0	0.4	-	-	0.5	-	-	-	-	-	-
Co	-	-	-	-	-	-	-	-	-	-	-	-	-	-	-	-
S	-	-	0.3	15.4	-	-	-	-	-	-	-	-	12.9	9.9	1.6	-
As	-	-	43.4	28.8	-	-	-	-	-	-	-	0.7	30.1	28.9	34.3	-
Sb	-	-	-	-	-	-	13.6	-	1.6	-	-	43.1	1.5	0.9	3.0	17.4
Bi	-	-	-	-	-	-	-	-	-	-	-	12.8	-	-	-	-
Sn	-	-	-	-	-	-	15.4	25.1	33.3	-	-	-	-	-	-	-
Total	99.4	101.0	100.1	99.9	100.1	100.0	99.1	99.6	100.0	99.6	100.7	98.4	99.8	99.8	97.6	100.0

Number	17	18	19	20	21	22	23	24	25	26	27	28	29	30	31
Sample	33	33	33	33	33	33	33	33	10/1	10/1	10/1	10/2	10/13	10/13	10/13
Pt	88.2	78.0	5.1	7.6	1.1	18.2	39.2	-	78.3	4.7	14.6	77.7	76.8	-	1.0
Pd	-	-	-	-	-	23.1	-	-	-	-	-	-	-	-	-
Rh	-	-	40.6	29.8	32.6	-	-	0.9	0.4	0.5	17.2	-	0.6	37.9	-
Ru	-	-	3.7	6.5	1.8	-	-	-	0.4	0.5	13.5	1.9	-	-	-
Ir	-	-	0.8	-	-	-	-	7.5	-	53.5	8.7	-	-	3.0	2.2
Os	-	-	-	-	-	-	-	-	-	1.8	2.6	-	-	-	0.8
Fe	11.1	15.5	1.3	1.7	2.2	2.0	3.3	29.2	13.8	0.5	1.4	16.0	16.9	4.6	6.0
Cu	-	3.0	-	-	-	-	0.4	-	4.2	-	-	2.7	2.4	-	0.9
Ni	0.4	2.1	-	-	-	-	-	23.6	2.3	-	-	2.6	2.3	23.6	51.7
Co	-	-	-	0.3	-	-	-	7.0	-	-	-	-	-	1.4	3.6
S	-	-	14.4	10.7	9.9	-	-	31.9	-	37.4	17.5	-	-	2.2	6.2
As	-	-	32.4	1.0	0.6	-	-	-	-	1.0	23.8	-	-	27.1	26.7
Sb	-	-	0.5	40.2	27.0	9.2	6.5	-	-	-	-	-	-	-	-
Bi	-	-	-	2.7	22.8	47.9	49.0	-	-	-	-	-	-	-	-
Sn	-	-	-	1.0	0.8	-	-	-	-	-	-	-	-	-	-
Total	99.7	98.6	98.8	101.5	98.8	100.4	98.4	100.1	99.4	99.9	99.3	100.9	99.0	99.8	99.1

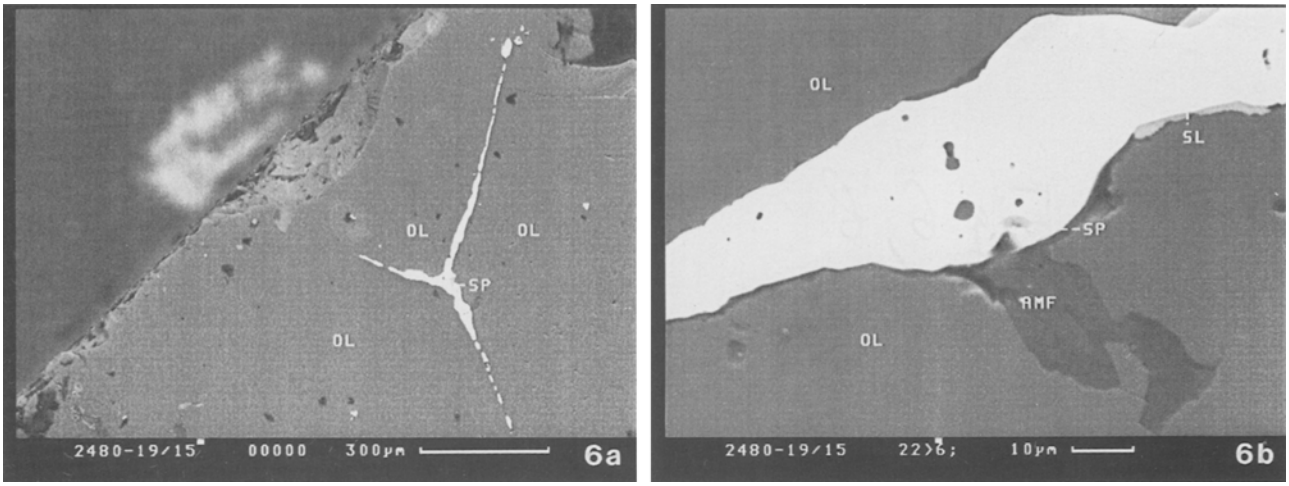

Fig. 6. Separation of chains of sperrylite "microdrops" at the joint of olivine grains. Sample 19, area 15. a) general view of the aggregate; b) detail: clinopyroxene (PIR) microglobules, enclosed in sperrylite (SP) are seen; SL sphalerite

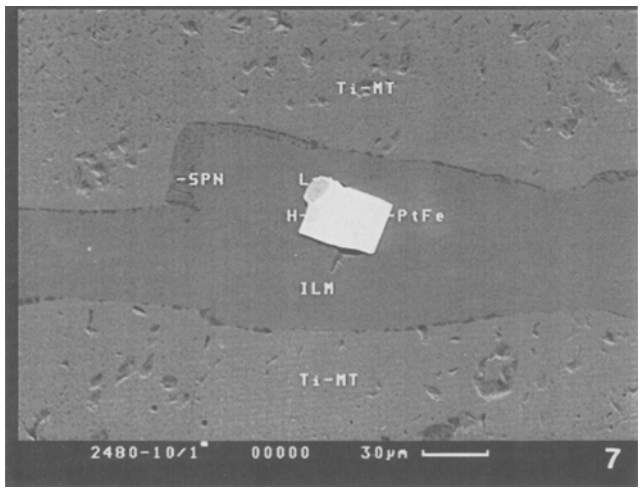

Fig. 7. PGM inclusion in titanomagnetite. Sample 10, site 1. PtFe tetraferroplatinum (?), H hollingworthite, L laurite, Ti-MT titanomagnetite, SPN spinel

and pentlandite. In sample 19, hollingworthite ((Rh, Ru, Pt, Fe)AsS, Table 3, analysis 4) and sperrylite ($PtAs_2$) were found in association with pentlandite, localized along the grain boundaries of olivine (Fig. 8a). The composition of pentlandite (Table 2, analysis 8) which rims a growth of PGM grains is close to that of the above described pentlandite, associated with amphiboles, chlorite, and magnetite (Table 2, analysis 9).

A composite PGM aggregate was found (sample 19) in close association with actinolite (Table 1, analysis 19) and magnetite (Table 1, analysis 20), localized along joints crossing grains of olivine (Fig. 8b). The PGM is an irregular grain of tetraferroplatinum (?) (Table 3, analysis 6) which contains very fine (1–6 μm) inclusions of cabriite ($(Pd, Pt)_2(Cu, Fe)(Sn, Sb)$, Table 3, analysis 7), Cu-rustenburgite ($(Pt, Pd, Cu, Fe)_3Sn$; Table 3, analysis 8), and an unnamed mineral ($(Pd, Pt)_4(Cu, Fe)_2(Sn, Sb)_3$; Table 3, analysis 9).

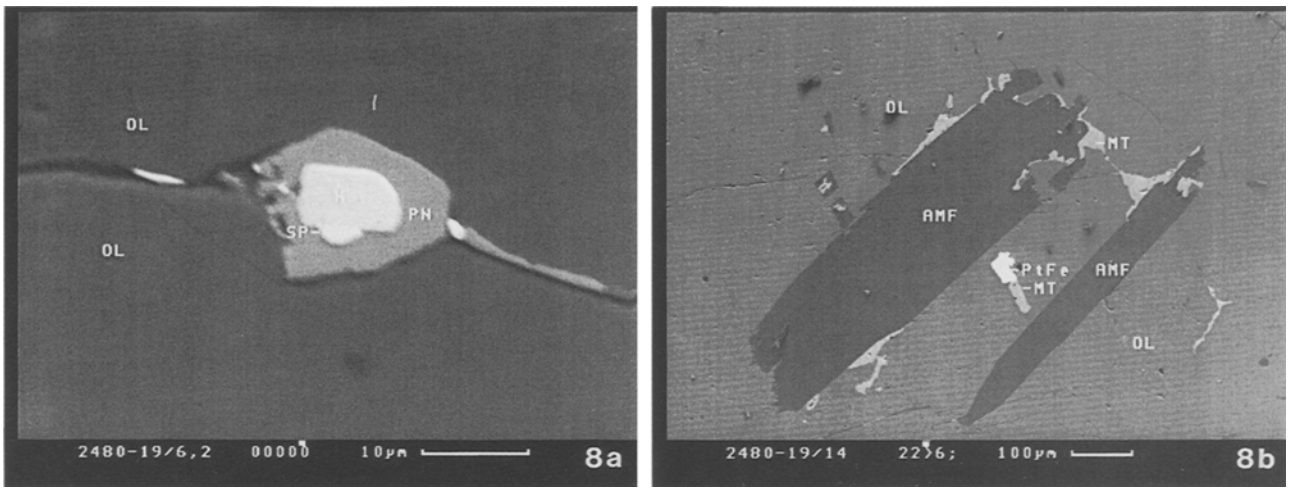

Fig. 8. PGM assemblages formed with minerals of the late chlorite-magnetite-amphibole assemblage of hortonolite dunites. Sample 19. a) area 6.2, b) area 14

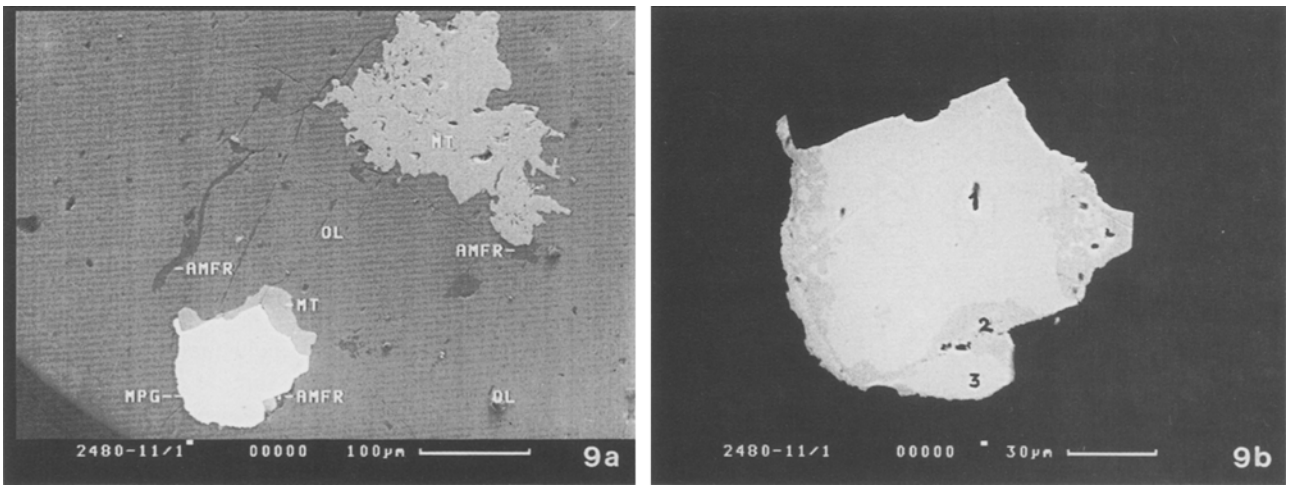

Fig. 9. Replacement of a primary inclusion of alloy (Pt, Fe) by tetraferroplatinum and associated PGM. Sample 11. a) general view of aggregate: it is seen that the PGM aggregate is accompanied by secondary magnetite and rhombic amphibole(?) which replace olivine; b) detail of Fig. 9a: 1 alloy (Pt, Fe), 2 tetraferroplatinum(?), 3 geversite

Fine (about 10 μm) irregular monomineralic separations of tetraferroplatinum (?) (Table 3, analysis 5) are also localized at the grain boundaries of olivine grains. The fact that Pt-Fe alloy inclusions in olivine and various tetraferroplatinum(?) assemblages formed at different times is unambiguously confirmed by replacement of crystals of earlier Pt-Fe alloy by tetraferroplatinum(?) and associated PGMs.

Both monomineralic occurrences of Pt-Fe alloy enclosed in nonbroken grains of olivine (Fig. 5) and PGM crystals (Table 3, analysis 10) replaced by tetraferroplatinum(?) (Table 3, analysis 11) and Bi-geversite ($(Pt, Sb, Bi)_2$; Table 3, analysis 12) around their periphery, were found in sample 11 (Fig. 9). It is noteworthy that PGM are accompanied here by aggregates of rhombic amphibole(?) and magnetite

replacing olivine. Additionally, very fine (1–3 μm) inclusions of hollingworthite ((Rh, Pt, Ir)AsS), platarsite ((Pt, Ir, Rh)AsS), sperrylite ($PtAs_2$), and an unnamed mineral ($(Pt, Ir, Fe)_3Sb$) were identified in the rim of tetraferroplatinum(?) (Table 3, analyses 13–16).

A practically complete pseudomorph of tetraferroplatinum(?) (Table 3, analysis 18) replacing a 35 by 40 μm crystal of Pt-Fe alloy was recognized in sample 33. The primary PGM (Table 3, analysis 17) is preserved in the grain only in the form of some fine (less than 5 μm) corroded relics. The pseudomorph occurs as ingrowths with magnetite and with Ru- and Rh-bearing pentlandite (Table 3, analysis 24). In addition, very fine (1–3 μm) inclusions of hollingworthite (RhAsS), Pt-Sb-sobolevskite(?) ((Pd, Pt, Fe)(Bi, Sb)), as well as unnamed minerals which have the following compositions: (Rh, Pt)SbS, (Rh, Fe)(Sb, Bi), and (Pt, Fe)(Bi, Sb) were identified in tetraferroplatinum(?) (Table 3, analyses 19–23).

Discussion

The sequence of PGM-forming processes can be reconstructed by analysis of the above paragenetic data from hortonolitic dunite mineral assemblages (silicates, oxides, sulfides, and PGM). This sequence must be correlated with the physical conditions of mineral formation observed at each stage in the formation of the pipes.

As pointed out above, the magmatic and metasomatic nature of platiniferous dunite pipes of the Bushveld Complex is debatable. In this connection it is interesting to note the occurrence of high-temperature pyroxene exsolution textures in dunites rich in pyroxene and titanomagnetite. According to estimates from single-pyroxene (*Mercier*, 1976) and two-pyroxene (*Lindsley*, 1983) geothermometry, blocking temperature values are in the range 980–1020 °C. With the use of previously described physico-chemical programs (GEO-CALC (*Perkins* et al., 1986) and THERIAK, worked by *D Kapitani* using data of *Berman* and *Brown* (1984)) the stability field of the mineral assemblage of hortonolitic dunites (olivine + clinopyroxene + orthopyroxene + magnetite + ilmenite (± phlogopite ± biotite)) is 960–680 °C, at a pressure greater than 8 kb. These calculations take into account nonideality and chemical composition of minerals in the presence of H_2O and CO_2.

Like sulfide microglobules (see Fig. 4), segregations of Pt-Fe alloy (see Fig. 5) may have been captured by crystallizing olivine grains. Hence, in terms of the paragenetic sequence, olivine and inclusion minerals can be classified with the earliest formed mineral assemblage of hortonolitic dunites. This conclusion is in line with the strong euhedral character of Pt-Fe alloy inclusions, and is confirmed by the find of an olivine ingrowth in a sulfide "microdrop" (see Fig. 4). Spatial dissociation of sulfide and early PGM inclusions in olivine should be noted. All the above facts can be explained in the light of known physico-chemical and experimental data, by proposing a magmatic origin for this mineral assemblage.

Studies of oceanic basalts (*Czamansky* and *Moore*, 1977; *Distler* et al., 1988) showed that sulfides are immiscible components of mafic magmas even at low concentrations of sulfur (about 0.1 wt.% and even under). Similar conclusions were also made from experimental evidence (*Haughton* et al., 1974). Assemblages of the studied sulfide "microdrops" (troilite + Fe-rich pentlandite + ferruginous chalcopyrite, and troilite + Fe-rich chalcopyrite) correspond to high-temperature compositions of primary sulfide phase, i.e. monosulfide solid solution poor in

nickel (Mss) and intermediate solid solution (Iss). Experimental findings suggest that similar compositions of the sulfide phase form in equilibrium with high-Fe silicate melt at low sulfur fugacities. By comparison with known differences in the composition of primary sulfides from mafic and ultramafic xenoliths in kimberlites (*Distler* et al., 1988), a low concentration of nickel in the primary sulfide phase from hortonolitic dunites suggests a mafic source of the parent magma of the dunite pipes.

Experiments show that solubility of all PGE's is insignificant in low-S high-Fe sulfide melt (Me/S = 1). Crystallization of such a melt rich in platinum leads to the formation of troilite, low in Pt, which coexists with Pt-Fe alloy, close to isoferroplatinum in component ratios (*Distler* et al., 1988). In the dunite pipes, low solubility of PGE's in silicate and low-S sulfide melts resulted in, on the one hand, their direct crystallization from the melt independently of segregations of primary sulfide phase (in the form of Pt-Fe alloy together with olivine or in the form of sperrylite together with clinopyroxene), and, on the other hand, concentration of PGE in fluid. An essential role of fluid even at the initial stages of the formation of dunite pipes is confirmed by the presence of minerals which contain alkalis and volatiles (biotite, amphiboles) in the "central" inclusions of sulfides and PGM in nonbroken grains of olivine. PGE's may have been transported and deposited with the aid of chlorides and, possibly, metal-organic compounds (*Schiffries*, 1982; *Stumpfl* and *Rucklidge*, 1982). These assumptions are supported by the presence of Cl-bearing minerals (apatite, hornblende, and others), as well as graphite in dunite pipes (*Stumpfl* and *Rucklidge*, 1982).

Analysis of the compositions and textural relationships of spinel exsolutions provides valuable information on the low-temperature stage of the enclosing rocks. PGM localization in ilmenite lamellae of titanomagnetitic concentrations in hortonolitic dunites (see Fig. 7) is a unique natural event which allows a relatively strict estimation of physico-chemical conditions of formation of these inclusions. Several successive stages occur in the titanomagnetite aggregates: first in the system magnetite-ulvöspinel-spinel, then magnetite-ulvöspinel, and finally oxidizing exsolution accompanied by ilmenite formation (see Fig. 2).

Experimental studies (*Lindsley*, 1976) showed that the position of the solvus in the system magnetite-ulvöspinel-spinel over a wide range of element contents varies between 800–1000 °C, whereas the solvus in the system ulvöspinel-magnetite is close to 500 °C. As a result, at the high-temperature stage, spinel (Zn-Cr-hercynite in the studied samples) exsolves from solid solution in the first system, leaving a matrix of solid solution magnetite-ulvöspinel. The lower temperature of the ulvöspinel-magnetite solvus results in a much finer exsolution texture as compared to the first stage. On fast cooling, such a solid solution can attain a chilled state as with dike rocks (*Price*, 1979). The size of the ulvöspinel lamellae in these samples (up to 3 μm in thickness) suggests a rather slow cooling of the hortonolitic dunites of the Onverwacht pipe.

Exsolution of ilmenite from titanomagnetite takes place due to its oxidation (*Buddington* and *Lindsley*, 1964), but is not the result of cooling of single-phase solid solution down to the temperature of a stable solvus as with the exsolution mechanism considered above. The compositions of coexisting ilmenite and titanomagnetite in sample 10 allow estimation of the oxygen fugacity and blocking temperatures at the time of exsolution (*Spencer* and *Lindsley*, 1981; *Stormer*, 1983). Trace element contents in the minerals were allowed for in calculations (Table 4). Fig. 10

Table 4. *Example of Estimation of T and fO_2 Values*

	TiMt 10/2H	Ilm 10/2H	TiMt 10/13	Ilm 10/13
SiO_2	0.19	-	0.18	0.08
TiO_2	8.75	52.62	4.95	50.71
Al_2O_3	2.79	-	0.67	0.62
V_2O_3	1.54	0.30	1.35	0.31
Cr_2O_3	2.67	-	1.13	-
Fe_2O_3	41.82	0.80	53.55	3.58
FeO	41.37	43.76	38.17	42.01
MnO	0.38	0.62	-	0.81
MgO	0.49	1.91	-	1.89
Si	0.007	-	0.007	0.002
Ti	0.246	0.985	0.142	0.948
Al	0.123	-	0.030	0.018
V	0.038	0.005	0.034	0.005
Cr	0.079	-	0.034	-
Fe^{3+}	1.176	0.015	1.536	0.067
Fe^{2+}	1.293	0.911	1.217	0.873
Mn	0.012	0.013	-	0.017
Mg	0.027	0.071	-	0.070
X_{ulv}	0.328		0.164	
X_{ilm}	0.992		0.964	
T°C	410		592	
$-\log(f_{O_2})$	33		21	

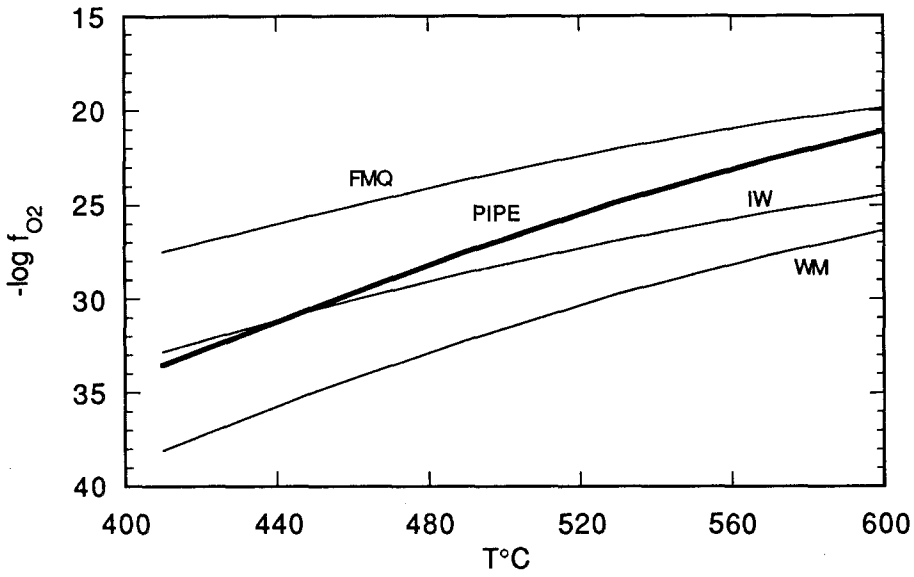

Fig. 10. $\log f_{O_2}$–T plot showing buffered cooling curve of ilmenite-titanomagnetite aggregate from hortonolite dunite

indicates that a subsolvus low-temperature (590–410 °C) mechanism under reducing conditions ($-\log f_{O_2} = 21$ and 33, respectively) was responsible for the formation of the observed assemblage of oxides and accessory PGM (tetraferroplatinum + laurite + hollingworthite and others). This conclusion is indirectly supported by the

presence of graphite in dunite pipes (*Stumpfl* and *Rucklidge*, 1982). The established temperature range of formation (1000–800°C to 400°C) and the texture of titanomagnetite aggregates indicate crystallization of residual magma rich in iron and a lengthy history of low-temperature "annealing" of titanomagnetite. This also explains the presence of inclusions—"microdrops" of sulfide in ilmenite lamellae; the inclusions are richer in copper than sulfide inclusions in olivine grains. Evolution of the high-temperature sulfide phase in equilibrium with silicate magma which is becoming progressively Cu-rich was observed, for instance, in oceanic basalts (*Czamansky* and *Moore*, 1977; *Distler* et al., 1988). A low rate of cooling of the system under study can be related to the elevated temperature of enclosing rocks at the time of intrusion of dunite pipes and/or to enrichment of residual melt in fluid. PGM and associated cobalt-pentlandite of inclusions in titanomagnetite probably crystallized from metalliferous fluid. It should be mentioned in this connection that cobalt-rich pentlandite was identified in accessories in the most fluidized rocks, for example, in kimberlites of Yakutia (*Distler* et al., 1988) or in alkaline rocks of the Tury Peninsula, USSR (*Bulakh* et al., 1975).

Further evolution of minerals of the dunite pipes may have been associated with intense autometasomatic reworking of the rocks under the influence of PGE-rich residual fluid. On decomposition of the fluid, PGM settled along the grain boundaries of olivine, along joints in the grains together with minerals of the later chlorite-magnetite-amphibole assemblage, as well as with ilmenite and pentlandite. Irregular forms of PGM grains of the assemblages and their extreme diversity, including both monomineralic grains of tetraferroplatinum(?) and complex aggregates composed of 6–7 PGM (tetraferroplatinum; Rh, Ir, Pt sulfarsenides; sperrylite; Pt, Pd, Sb, Bi, Sn minerals, and others), agree with this model of ore deposition at this stage of mineral formation.

Experimental studies enable us to determine the formation temperature of some mineral assemblages. For instance, the aggregate of tetraferroplatinum(?), cabriite ($(Pd, Pt)_2(Cu, Fe)(Sn, Sb)$), Cu-rustenburgite ($(Pt, Pd, Cu, Fe)_3Sb$), and unnamed mineral ($(Pd, Pt)_4(Cu, Fe)_2(Sn, Sb)_3$) may have been formed at temperatures below 300 °C. Studies of the pseudobinary section Pd_3Sn–Cu_3Sn in the system Pd–Sn–Cu–HCl (*Distler* et al., 1988) showed that at a temperature above 300 °C only binary stannides of palladium with a low copper content crystallize, and the compound Pd_2SnCu—an analog of cabriite—is stable at temperatures only below 100 °C.

The predominant development of the late PGM assemblages was shown by the advantageous use of black amphibole accumulations as ore guides in platinum mining in dunite pipes (*Wagner*, 1929; *Stumpfl* and *Rucklidge*, 1982). Finally, the known PGM aureole of the "pipe-like" type in the Merensky Reef (*Peyerl*, 1982) convincingly confirms intense generation of platiniferous fluid by dunite pipes.

Conclusions

1) Several PGM assemblages were identified in the Mooihoek and Onverwacht pipes. These assemblages formed at different stages, and can be related to the formation of the main rock-forming minerals of the hortonolitic dunites: a) (Pt, Fe) alloy similar to isoferroplatinum in composition, syngenetic with olivine; b) sperrylite syngenetic with clinopyroxene; c) tetraferroplatinum(?), laurite, hollingworthite, unnamed mineral ((Rh, Ru)NiAs), syngenetic with titanomagnetite; and d) tetra-

ferroplatinum(?), sperrylite, geversite, hollingworthite, platarsite, cabriite, rustenburgite, sobolevskite(?), unnamed minerals $(Pd, Pt)_4(Cu, Fe)_2(Sn, Sb)_3$, $(Pt, Ir)_3Sb$, (Rh, Ir, Pt)SbS, Rh(Sb, Bi), and Pt(Bi, Sb), syngenetic with amphiboles, magnetite, chlorite, ilmenite and pentlandite.

2) Fine (less than 0.1 mm) drop-shaped inclusions, consisting of troilite, Fe-rich chalcopyrite, and Fe-rich pentlandite were recognized in grains of olivine; the inclusions correspond to compositions of the high-temperature nickel-poor sulfide phase, in equilibrium with high-Fe silicate melt at conditions of low sulfur fugacity.

3) PGE-rich hortonolitic dunites underwent, partly at least, a magmatic stage, followed by a prolonged stage of subsolidus autometasomatic transformations under the influence of metalliferous (PGE-rich) fluid.

4) Low solubility of PGEs in silicate and low-S sulfide melts resulted in, on the one hand, direct crystallization of PGM from the melt independently of segregation of the primary sulfide phase, and, on the other hand, concentration of PGE in fluid. PGE-rich fluid generated numerous PGM assemblages both from the crystallization of residual magma which concentrated Fe and Ti, and as a result of intense autometasomatic reworking of primary hortonolitic dunites.

Acknowledgements

The authors are sincerely grateful to *B. Saini-Eidukat* for invaluable help in preparing the report for publication in English. The constructive comments of an anonymous reviewer have been invaluable.

References

Berman RG, Brown TH (1984) A thermodynamic model for multicomponent melts, with application to the system $CaO–Al_2O_3–SiO_2$. Geochim Cosmochim Acta 48: 661–678

Bowles JFW (1990) Platinum-iron alloys, their structural and magnetic characteristics in relation to hydrothermal and low-temperature genesis. Mineral and Petrol 43: 37–47

Buddington AF, Lindsley DH (1964) Iron titanium oxide minerals and synthetic equivalents. Journ Petrol 5: 310–316

Bulakh AG, Evdokimov MD, Rudashevsky NS (1975) Distribution patterns of Ni and Co in ultrabasic alkaline rocks and carbonatites of the Tury Peninsula. Geokhimiya 5: 733–739 (in Russian)

Cabri LJ (1977b) Platinum-group minerals from Onverwacht.III. Genkinite $(Pt, Pd)_4Sb_3$, a new mineral. Canad Mineral 15: 389–392

— *Feather CE* (1975) Platinum-iron alloys: a nomenclature based on a study of natural and synthetic alloys. Canad Mineral 13: 117–126

— *Laflamme JMG, Stewart JM* (1977 a) Platinum-group minerals from Onverwacht.II. Platarsite, a new sulfarsenide of platinum. Canad Mineral 15: 385–388

Cameron EN, Desborough GA (1964) Origin of certain magnetite-bearing pegmatites in the eastern part of the Bushveld Complex, South Africa. Econ Geol 59: 197–225

Czamansky GK, Moore JG (1977) Composition and phase chemistry of sulfide globules in basalt from Mid-Atlantic Ridge rift Valley near 37° latitude. Bull Geol Soc Am 88: 587–599

Distler VV et al. (1988) Petrology of sulfide magmatic ore formation. Nauka, Moscow: 232 pp (in Russian)

Duke JM (1980) Platinum metals in magmatic sulfides ores. Science 208: 1417–1424

Haughton DR, Roeder PL, Skinner BJ (1974) Solubility of sulfur in mafic magmas. Econ Geol 69: 451–467

Karpenkov AM et al. (1974) Iron-rich variety of chalcopyrite. Zapiski Vsesoyuznogo Mineralogicheskogo Obshchestva 5: 601–606 (in Russian)

Lindsley DH (1976) Experimental studies of oxide minerals. In: Rumble D (ed.) Oxide minerals Miner Soc Am Short Course Notes

Lindsley DH (1983) Pyroxene thermometry. Am Mineral 68: 477–493

Mercier JCC (1976) Single-pyroxene geothermometry and geobarometry. Am Mineral 61: 603–615

Naldrett AJ, Cabri Li (1976) Ultramafic and related mafic rocks: their classification and genesis with special reference to the concentration of nickel sulfides and platinum-group elements. Econ Geol 71: 1131–1158

Perkins EH, Brown TH, Berman RG (1986) PTX-System: three programs for calculation of pressure-temperature-composition phase diagrams. Computers & Geosciences 12: 749–755

Peyerl W (1982) The influence of the Driekop dunite pipe on the platinum-group mineralogy of the UG-2 chromite in its vicinity. Econ Geol 77: 1432–1438

Price GD (1979) Microstructures in titanomagnetites as guide to cooling rates of a Swedish intrusion. Geol mag 116: 313–317

Spencer KJ, Lindsley DH (1981) A solution model for coexisting iron-titanium oxides. Am Mineral 66: 1189–1201

Stormer JC, Jr (1983) The effect of recalculation on estimates of temperature and oxygen fugacity from analyses of multicomponent iron-titanium oxides. Am Mineral 68: 586–594

Stumpfl EF (1961) Some new platinoid-rich minerals, identified with the electron microanalyzer. Mineral Mag 32: 833–847

— (1962) Some aspects of the genesis of platinum deposits. Econ Geol 57: 619–623

— *Clark AM* (1965) Hollingworthite, a new rhodium mineral, identified by electron probe microanalysis. Am Mineral 50: 1068–1074

— *Rucklidge JC* (1982) The platiniferous dunite pipes of the Eastern Bushveld. Econ Geol 77: 1419–1431

— *Tarkian M* (1976) Platinum genesis: new mineralogical evidence. Econ Geol 71: 1451–1460

von Gruenewaldt G (1979) A review of recent concepts of the Bushveld Complex with particular reference to sulfide mineralization. Canad Mineral 17: 233–256

Wagner PA (1929) The platinum deposits and mines of South Africa. Edinburgh, Oliver and Boyd: 326 p

Authors' Addresses: Prof. N. S. Rudashevsky, Mechanobr Centre for Chemical and Physical Research, 21 Line 8A, St. Petersburg 199026, Russia; Dr. S. N. Avdontsev, All-Union Geological Research Institute, St. Petersburg 199026, Russia; Dr. M. B. Dneprovskaya, Central Geological Exploration Museum, St. Petersburg, Russia.